Edited by
Ghenadii Korotcenkov

POROUS SILICON

From Formation to Application

Formation and Properties, Volume One

CRC Press

Fundamentals of Silicon Porosification via Electrochemical Etching

2

Enrique Quiroga-González and Helmut Föll

CONTENTS

We nucleated as a couple,

and at the right time we branched.

With love, to my wife and children.

2.1 INTRODUCTION

Since the discovery of the interesting luminescent properties of microporous Si (Canham 1990; Lehmann and Gösele 1991), and controllable macropore etching under illumination in *n*-type silicon (Lehmann and Föll 1990), the development of porous Si systems has exponentially increased. In this regard, nowadays Si can be etched in a controlled manner, with lithiographically defined or undefined (random) patterns. Additionally, silicon can be electrochemically etched in various electrolytes, like HF-based solutions with fluorides (Hoffmann et al. 2000) and KOH-based (Mathwig et al. 2011) solutions. This chapter will deal with the basics of porosification, centering the discussion on the most common and successful etching system, the Si-HF system.

2.2 ELECTROCHEMISTRY OF SILICON. ELECTROCHEMICAL REACTIONS IN THE SILICON SYSTEM

2.2.1 ELECTROCHEMICAL ETCHING SYSTEM FOR Si

An electrochemical system for performing electrochemical etching of Si consists of the components schematized in Figure 2.1: (a) anode electrode, which is the Si piece to be etched; (b) cathode electrode, usually made of Pt, which is not corroded during the etching process; (c) electrolyte, which enables the ionic transport from the cathode to the anode, and contains etching species; and (d) reference electrode, which can be any standard electrode used as reference (Ag/AgCl, saturated calomel, etc.), or a noble metal like Pt (pseudo-reference). The reference electrode is positioned close to the samples to be etched, to keep the contribution of the electrolyte in the voltage measurements as small as possible.

In the etching system of Figure 2.1, the Si piece is at the bottom, making contact with the electrolyte through a hole in a container (commonly sealed with an O-ring). This is the simplest and usual way of arranging the system, to assure that the electrolyte will always make a homogeneous contact with Si, even when it is available in small quantities. A good material for fabricating the container is Teflon because it is chemically stable even in very concentrated HF solutions.

Optionally, but preferably, the etching system may also have a temperature control and an electrolyte pumping system (Christophersen et al. 2000a, 2001). A temperature control is important because the diffusion of the etchant and the semiconductor electrical properties greatly depend on the temperature. The pumping system avoids problems like electrolyte depletion at the

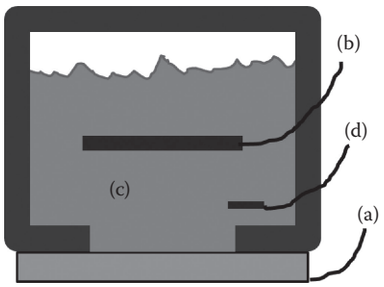

FIGURE 2.1 Electrochemical etching system. (a) Si sample (working electrode); (b) counter electrode, made of Pt; (c) electrolyte (etchant); and (d) reference electrode.

interface but adds certain degrees of anisotropy due to the electrolyte flow direction. The uniform processing of large samples like complete wafers requires considerable sophistication in the set-up. See, for example, the system developed by Föll et al. (2002).

2.2.2 CURRENT-VOLTAGE CHARACTERISTICS

The electrical behavior of the electrochemical etching system behaves in a first approximation like a rectifying metal-semiconductor contact known as Schottky contact. Typical I-V curves (current-voltage characteristics) of an electrochemical Si etching system using HF-based aqueous electrolytes is shown in Figures 2.2 and 2.3 for *p*-type and *n*-type Si, respectively. The area of contact of the electrolyte with Si is defined by the etching cell, and is variable from cell to cell. Thus, it is important to use "current density" (J) instead of the current I in all measurements and figures. Accounts that are far more detailed can be found in Lehmann (2002) and Kochergin and Föll (2009).

While the *J-V* curves of the *p*- and *n*-type Si etching systems in the anodic region show some forward or reverse diode-like characteristics, respectively, there are some special features never encountered in solid-state junctions. Si may dissolve with time, invariably leading to changes in the *J-V* characteristics with time. The most important features of the $J(V)$ characteristics not observed for solid state diodes are the peaks PSL (porous Si layer) at current density J_{PSL}, the

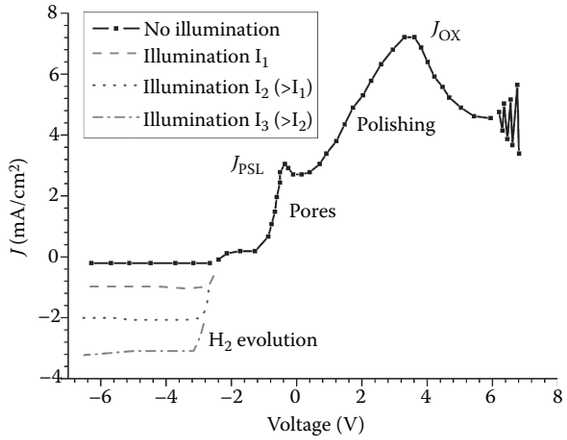

FIGURE 2.2 Current–voltage (I-V) characteristics of a *p*-type Si–(HF-based) electrolyte system.

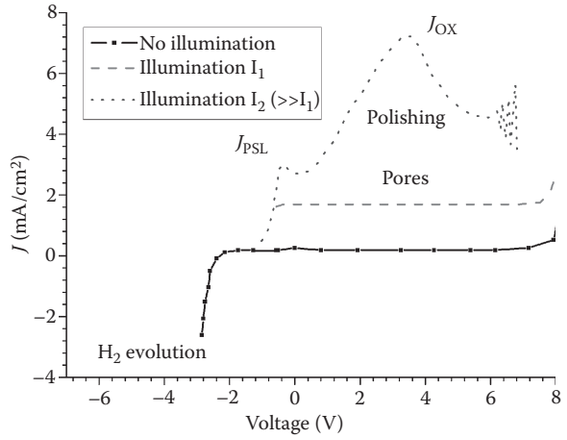

FIGURE 2.3 Current–Voltage (I-V) characteristics of an *n*-type Si–(HF-based) electrolyte system. Pores can be obtained just under illumination.

"oxide peak" at J_{OX}, and current oscillations at high voltages (see Figures 2.2 and 2.3). In the case of n-Si, anodic currents need illumination, and the major deviation from a normal diode behavior is the strong nonlinearity of the response to light for current densities approaching or exceeding J_{PSL}.

A strong cathodic biasing of Si (forward bias for *n*-type and reverse bias for *p*-type) allows an easy transfer of electrons to the electrolyte. The electron transfer then produces H_2 evolution on the cathode side ($2H^+ + 2e^- \rightarrow H_2$). On the other hand, an anodic biasing will result in Si dissolution. This process requires electronic holes, thus, in *n*-type Si, for an appreciable Si dissolution, it is necessary to apply light to generate electron-hole pairs. The different sections of the *J-V* curves will be described and explained in the following points, going from negative to positive voltages:

1. The cathodic part of the *J-V* curves for both *p*- and *n*-type Si behaves as expected for a reverse bias in a solid-state junction. For *n*-type Si, the electrolyte-Si junction is in forward condition; the current grows exponentially with the applied voltage and essentially generates H_2. On the other hand, for *p*-type Si in equilibrium, the reverse current is of low intensity, and it is necessary to apply large voltages to be able to observe breakdown currents. Illuminating *p*-type Si, the current increases proportionally to the illumination intensity. An increase in the current produced by light (photocurrent) translates into an increase of H_2 generation, which is uninteresting when talking about microstructuring of semiconductors.
2. At around 0 A/cm^2 it is interesting that the voltage is not 0 V. Some "built-in" voltage depends on the nature of the reference electrode (and the surface condition of the Si sample). The needed voltages to drive some (forward) current through the etching system greatly depend on the kind of reactions taking place at the electrodes. H_2 evolution from HF-containing solutions needs a certain minimum (negative) "overpotential."
3. On the anodic side (i.e., positive currents), Si is always dissolved when using HF-containing electrolytes. Because of this, the surface of the Si electrode changes with time. It may at the extremes become polished or porous. This causes changes in the *J-V* characteristics with time because not only is $J(V)$ small between pores and large inside pores, but also the Si area changes by orders of magnitude with time. This area change is usually neglected in calculating current densities where always the nominal area is used; nevertheless, it is of prime importance for understanding the mechanisms of pore formation.

In *p*-type Si, pores are produced in the voltage region below the *PSL* peak; typically, micropores for large current densities and macropores for lower ones. Details depend on the resistivity, the nature of the electrolyte, and the cell design, and cannot easily be generalized. When one goes beyond this limit, electropolishing is observed, and going even beyond the J_{OX} peak, the polishing is always accompanied by self-induced current oscillations under potentiostatic conditions, and voltage oscillations under galvanostatic conditions. These oscillations are obvious examples of self-organized phenomena in semiconductor electrochemistry, expressing themselves as current oscillations in time. However, pore formation per definition involves a kind of current oscillation in space and thus is a self-organization feature just as well (Föll 1991).

In *n*-type Si under darkness conditions, the anodic *J-V* characteristics are those for a reverse-biased junction (the current is very small), as expected. However, if illumination is applied, the current intensity increases, dissolving Si. At intermediate illumination intensities, pores are produced, independently of the voltage. Furthermore, if the illumination intensity is so high that the reaction limited maximum current density is smaller than the induced photocurrent. The *J-V* characteristics look very similar to that of *p*-type Si (dotted curve of Figure 2.3); thus, the same regions of porosification and electropolishing are observed when the voltage is varied.

"if the illumination intensity is so..." this sentence is incomplete. Please rewrite.

It is worthwhile to mention that any "working point" (i.e., the initially defined external current and voltage pair [*J*, *V*]) for *p*-type Si is confined in the *J-V* curve of the system. In contrast, for *n*-type Si, any working point below the limiting curve for intense illumination can be chosen by simply providing suitable illumination conditions. In other words, for *p*-type Si there is only one free (prime) parameter (voltage or current), whereas for *n*-type Si there are three: voltage, current, and illumination intensity, two of which can be independently varied in principle (and within certain limits, of course).

Finally, it should be mentioned that the I-V curves shown in Figures 2.2 and 2.3 may vary depending on the level of doping of Si (e.g., *p*, *p*+, *p*++, or *n*, *n*+, *n*++) (Zhang 2001; Lehmann 2002).

The same is true if one uses different solvents than water (DMA, DMF, DMSO, etc.) (Propst and Kohl 1994; Propst et al. 1994; Föll et al. 2002), and different HF concentrations.

2.3 Si ETCHING. CHEMICAL REACTIONS GOVERNING THE DISSOLUTION OF SILICON

Electrochemical etching of Si consists of any combinations of the following four different net chemical reactions (cf., e.g., Föll et al. 2002 for a detailed discussion):

2.3.1 DIRECT DISSOLUTION OF Si

(2.1) $$\mathrm{Si} + x h^+ - y e^- \rightarrow \mathrm{Si}^{4+}$$

where x holes (h^+), with x being ≥1, are consumed in the reactions together with y injected electrons (e^-) that contribute with the rest of the charge needed. This kind of dissolution makes the most efficient use of holes because it can be triggered even by only one hole.

In the case of etching in HF-containing solutions, the reaction turns to be (Anglin et al. 2008):

(2.2) $$\mathrm{Si} + 6\mathrm{F}^- + 2\mathrm{H}^+ + 2h^+ \rightarrow \mathrm{SiF}_6^{2-} + \mathrm{H}_2$$

which is a 2-hole process, producing an Si compound where the Si valence is 4+, as described in the general Equation 2.1. This is usually called divalent dissolution, due to the amount of necessary charges for the process (Lehmann and Gösele 1991). As described in Equation 2.1, direct dissolution could have any valence between 1 and 4; however, in most of the cases, it occurs with a valence of around 2. The final product of the etching process is the stable complex $\left[2\mathrm{H}^+ - \mathrm{SiF}_6^{2-}\right]$, or $\mathrm{H_2SiF_6}$.

Direct dissolution consumes HF and liberates hydrogen ($\mathrm{H_2}$), but in the intermediate reactions, there is the occurrence of H^+. This gives a strong hint that the reaction rate might be sensitive to the pH value of the electrolyte and that local reactions (e.g., at a pore tip) may locally change the pH value of the electrolyte.

2.3.2 OXIDATION OF Si

The oxidation process of Si can be described by the net reaction:

(2.3) $$\mathrm{Si} + 4h^+ + 2\mathrm{O}^{2-} \rightarrow \mathrm{SiO_2}$$

Should this be Equation 2.3?

As can be observed in Equation 2.2, four holes participate in the oxidation process. In the presence of water, the oxidation reaction can be written as (Huang et al. 2011):

(2.4) $$\mathrm{Si} + 2\mathrm{H_2O} + 4h^+ \rightarrow \mathrm{SiO_2} + 4\mathrm{H}^+ + 4e^-$$

Much simplified, this process occurs if the current density HF diffusion. As in this regime, the available HF concentration is lower than the amount of water, the water molecules take the role of nucleophile, forming Si-O bonds (Sailor 2012).

" this process occurs if the current..." sentence is incomplete. Please rewrite.

2.3.3 OXIDE DISSOLUTION

In the voltage range of porosification, the Si oxide dissolution process occurs mainly chemically, with no electric current involved. The net reaction can be written as Equation 2.5:

(2.5) $$\mathrm{SiO_2} + 6\mathrm{F}^- + 6\mathrm{H}^+ \rightarrow \mathrm{H_2SiF_6} + 2\mathrm{H_2O}$$

This process couples to the oxide formation and essentially limits the total current density that the system can process because the oxide generation rate cannot be larger than the dissolution rate (on average). The only exceptions are the somewhat exotic but not necessarily rare cases where the oxide does not dissolve but fractures off mechanically due to stress levels increasing with oxide thickness (Parkhutik 1999). The combined process of oxidation and oxide dissolution is known as tetravalent Si dissolution, since four holes are needed.

2.3.4 HYDROGEN TERMINATION OF THE Si SURFACE

The coverage of the free Si surface can be formally described by the chemical Equation 2.6:

$$\mathrm{Si}^{x} + x\mathrm{H}^{+} \rightarrow \mathrm{SiH}_{x} \tag{2.6}$$

where x is the number of open covalent bonds on the Si surface (number of defects per Si atom). When Si is etched in HF-based solutions, the surface dangling bonds become terminated with H atoms (including the H atoms of alcohol or surfactant molecules). It is known through XPS and FTIR studies that hydrides like SiH, SiH_2, and SiH_3 are formed (Chabal et al. 1983; Yavlonovitch et al. 1986); that is why the chemical formula SiH_x is used in Equation 2.6. The hydrogen termination of the surface states can be considered a passivation process, which is governed by a reaction constant. This removal of interface states is important because they introduce a certain density of states in the band-gap of the Si (Sailor 2012). The rate of passivation depends on parameters like crystal orientation, temperature, and etchant composition.

In typical pore growth situations, the dissolution of Si is a combination of divalent (direct Si dissolution) and tetravalent (dissolution of Si through the formation and dissolution of SiO_2). During pore formation, current flows per definition almost exclusively through the pore tip and not through the pore walls. Most of the pore surface thus must be passivated with hydrogen. The quality of this passivation determines the residual flow of current to the pore walls and consequently the enlargement of pore diameters henceforth called electrochemical "over-etching."

The four described processes are all present during Si etching. Nevertheless, they cannot by definition occur all at the same time and at the same small place increment; thus, a totally homogeneous current flow is intrinsically impossible (Föll et al. 2002). The question will be if the averages observed on a macroscopic scale are constant in time and space (producing "polishing"), constant in space but not in time (producing polishing with externally observable current/voltage oscillations), constant in time but not in space (producing pores or current oscillations in space but constant external parameters), or not at all (producing "chaos," including coupled oscillations in space and time).

2.4 MECHANISM OF Si POROSIFICATION DURING ANODIC ETCHING (FROM MESO- AND MICROPOROUS Si TO MACROPOROUS Si)

When talking about electrochemical pore etching in Si, a wide variety of pore diameters can be considered, from a few nanometers to tens of micrometers. Additionally, a huge range of geometries and morphologies can also be encountered. In this respect, it is hard to describe the structure of porous Si in a simple manner. However, there is a standard definition of pores considering the pore diameter only: the IUPAC convention. According to IUPAC, pores can be grouped into micropores (diameter <2 nm), mesopores (diameter 2–50 nm), and macropores (diameter >50 nm).

Even though, the name "nanopores" has been lately used to describe pores with at least one dimension smaller than 100 nm, it is not an officially accepted definition. Additionally, a plethora of nonstandardized names are used to describe the pores according to their morphology (branched pores, tree-like pores, nano-sponge, etc.), their formation mechanism (e.g., break-down pores), or their orientation (crystallographic pores and current-line pores) (cf., e.g., Kochergin and Föll 2009).

In this section, the mechanisms for the electrochemical porosification of Si in micro-, meso-, and macropores will be discussed.

2.4.1 PORE FORMATION MODELS

There is no generally accepted electrochemical pore formation mechanism model for Si (or other semiconductors) and what there is has no or very limited predictive power. The Si anodic porosification is a complicated process that mixes electronic, fluidic, and chemical factors. A wide range of externally accessible parameters has to be taken into account when electrochemically etching pores in Si: electrolyte composition, doping type and concentration in Si, minority carrier lifetime and lifetime uniformity, Si crystal orientation, Si sample preconditioning/patterning, applied voltage/current, temperature, illumination conditions, backside contact quality, and electrolyte flow rate. All these parameters play a role, and may affect in a higher or lower scale the porosification. In addition, the nucleation of pores is absolutely crucial and influenced critically by, for example, perfection of the lithography for "seeded" pores and perfection of the surface and starting conditions during the first few seconds/minutes of the experiment for "random" pores. Indeed, producing a uniform array of random pores usually calls for special conditions (e.g., high potential) during the pore initiation part of the experiment.

No wonder that the porous Si samples prepared by different research groups are not comparable, even for nominally identical conditions. This produces a major problem for considering mechanisms of pore formation. Nevertheless, some common features of the porosification process are known, mainly evidenced through experimental observations. Based on some points from Sailor (2012), the main features of the Si electrochemical porosification process can be summarized in the following: (1) Unless the Si wafer has been specifically prepatterned, in most of the cases the pores nucleate homogeneously with no apparent order on the Si surface; although there are some examples of self-organization by certain etching conditions (Föll et al. 2006). (2) Current by necessity flows preferentially at the pore tips and the pore walls passivate (to a certain degree, as will become clear later in this section). (3) Once formed, the pores do not rearrange.

There are different models trying to explain the pore formation in different length scales, at different growth stages. Three groups of models can be made (Parkhutik 1999):

1. Models for pore nucleation
2. Models for stationary pore growth
3. Models trying to explain the whole pore growth process

2.4.1.1 MODELS FOR PORE NUCLEATION

A solid representative of the first group of models is the one proposed by Kang and Jorné (1993). The nucleation of pores at the silicon surface is treated mathematically as a phenomenon of instability of a planar surface toward small perturbations. The model considers that the electron holes migrate to the surface of the semiconductor, and the F^- ions from the HF-based etchant diffuse to the electrolyte-semiconductor interface. Due to the applied voltage, there exist some small perturbations at the Si surface, which can be modeled as Fourier components of the form $y = \alpha\exp(i\omega x + \beta t)$, where ω is a spatial frequency along the perturbed surface and β is the rate of development of the perturbation. α is the amplitude of the perturbation. At making an analysis of stability, certain frequencies ω_{max} are found for the maximum values of β. According to this, there should be some characteristic eigenvalues for the preferential distance between pores, for a given set of experimental conditions. The prediction of this model is that the distance between pores varies with the square root of the applied voltage. This prediction is not surprising because it mirrors the behavior of a solid state junction, ruled by Poisson's equation.

The width of the junction or space charge region length (SCRL) is given by:

$$\mathrm{SCRL} = \sqrt{\frac{2\varepsilon V}{qN}}, \tag{2.7}$$

where ε is the dielectric constant of Si, V is the applied voltage, q is the charge of electrons, and N is the doping concentration.

Another form of pore nucleation is through mechanical stress (cracks) and defects on the Si surface. These points work as easy paths for pore propagation (Parkhutik and Andrade Ibarra 1999). There is, however, no clear example for this kind of pore nucleation and it plays a minor role at best. It is also possible to introduce defects intentionally in regular arrays; pores nucleate at those defects as long as the distances between defects is not too large or small. That is, in short, what lithography aims to achieve.

Additional mechanisms of pore nucleation are saturation of vacancies at the surface (Corbett et al. 1995), surface tension (Kompan et al. 1996), and general pattern formation by current flow inhomogeneity in space (Carstensen et al. 1998, 1999).

2.4.1.2 MODELS FOR STATIONARY PORE GROWTH

Lehmann and Föll (1990) were the first to propose a macropore formation and growth model that centered on the SCRL. The model in its final form (Lehmann 1993) assumes that the local current density is always constant and is given by J_{PSL}, which is the major parameter governing pore geometry and morphology. The model does have some predictive power demonstrated by the fact that it was used to produce n-macropores for the first time. The model has been experimentally validated to some extent for macropore formation (Lehmann 1993). It is clear that the SCRL is very important for pore growth, even though it has become obvious that the SCRL is not sufficient to explain the formation of pores in general (Hejjo Al Rifai et al. 2000).

The SCRL is the central part of Lehmann's model (Lehmann 1993; Lehmann and Grüning 1997) for describing macropore formation in *n*-type Si. As for etching *n*-type material, generation of carriers with light is needed, the model considers that the current flowing through the pore tips during the etching process is mainly the photocurrent. The small dark or leakage current also flows through the pore wall, increasing the pore size with time and thus rendering the pores slightly conical in appearance. The "Lehmann formula" relates the pore diameter (d) with the (average) lattice constant (a) of the pore array and the total current density (J) applied during the etching:

$$\left(\frac{d}{a}\right)^2 = \frac{J}{J_{PSL}} \tag{2.8}$$

The pores have the freedom to adjust themselves to the diameters and distances for obtaining J_{PSL} in all the active areas (= pore tips) during etching. If the Si wafers are pre-structured, all pores will do the same; if not, some randomizations occur where the average distance between pores is given by 2SCRL and the pore diameters adjust accordingly. The model considers that the pore walls are passivated against the holes produced by illumination due to the space charge region. However, the SCR does not passivate against holes generated in that region (i.e., the dark current), and holes from the illumination may penetrate under certain circumstances. One reason for this is the introduction of charged surface states during the etching process.

A similar model, which is a particularization for the case of microporous Si, is the "quantum wire model" (Lehmann and Gösele 1991). It postulates that there is quantum confinement for carriers at the pore walls due to their very small thickness (in the range of nanometers). Due to this, the penetration of electrons or holes to the pore walls becomes more difficult, and can be thought of as passivated. The dissolution of the pore walls is inhibited, stabilizing the pore structure. The model defines accurately the minimum distance between micropores; however, it has nothing to say about the diameter of the pores itself.

One of the first models in providing a quantitative estimation of the pore geometry for mesopores produced by SCR failing was proposed by Beale et al. (1985). It considers that a Schottky-type barrier at the Si-electrolyte interface held at reverse conditions can be overcome by breakdown. The electron transport through the barrier is produced either by tunneling in the case of heavily doped Si or by Schottky emission in the case of lower doping. In the model, the pore tips are semispherical. The current is considered to flow preferentially at these points because the electric field is concentrated there, while the barrier height is lowered. The contribution of this model is simply the differentiation in transport mechanisms between heavily and lightly doped Si, which produce different characteristic pore sizes.

The model proposed by Zhang (1991) considers that pore growth occurs through two competing processes: anodic oxide formation and further dissolution in the HF-based electrolyte, and direct anodic dissolution of Si. The probability of occurrence of the one or the other process highly depends on the applied electric field strength and thus potential and current density. The first process mainly occurs at higher field strengths. On the other hand, it is considered that the current density and the doping concentration determine the pore morphology; these variables influence the height of the potential barrier at the pore tips, and consequently the electron tunneling probability (the carrier transport mechanism).

2.4.1.3 MODELS EXPLAINING THE WHOLE GROWTH PROCESS

A highly developed model for pore growth, including the stochastic nature of pore geometries and morphologies, is the "current burst model" (CBM), proposed by Föll et al. (2002). The model postulates that there are definite correlations between the four different processes occurring during the anodization of Si (see Section 2.3). It has three main postulates:

1. The current mostly flows inhomogenously through an Si sample both in time and space. There are times when no charge is transferred across some areas. The charge transfer occurs at some points of space and time (x, y, t) on the Si surface with some probability p(x, y, t) that depends on the surface state S(x, y, t), having an intrinsically stochastic probability nature. Every charge transfer event is called current burst (CB).
2. The sequence of processes occurring during a current burst is dictated by logic. On a "free" Si surface, direct dissolution of Si starts the current flow, followed by oxidation, leading to passivation and thus stop of current flow. The next CB has to wait until the oxide has been sufficiently dissolved. Hydrogen–passivation may produce a similar effect than oxidation. Figure 2.4 shows an example of two consecutive current bursts, indicating each of the processes occurring.
3. An interaction between individual CBs may occur in both space and time. This means that the nucleation probability p(x, y, t) of a CB does not only depend on S(x, y, t), but also on what has happened before (S[x, y, t_0]) and on what is going on in the neighborhood. Interactions in space may result in a correlation in time, and when there is a correlation in time, current or voltage oscillations result. Interactions in time produce pores.

The model is quantitative in principle and can account for all voltage and current oscillations quantitatively, applying a Monte-Carlo computer simulation (Föll et al. 2011). Simulation of pore formation is presently limited by the available computing power because it needs to consider large areas and is, by definition, three-dimensional.

The model works quite well in a semiquantitative way for describing the formation of different kinds of pores, depending on the kind of spatio-temporal correlations. It has predicted new kinds

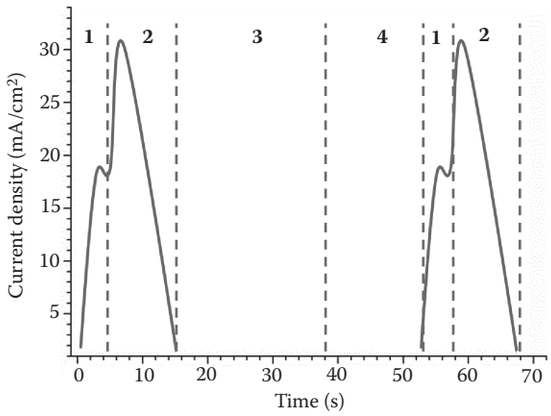

FIGURE 2.4 Two consecutive current bursts. They consist of a series of events: (1) Direct dissolution of Si, (2) oxidation of Si, (3) Si oxide dissolution, and (4) H_2 passivation.

of pores that were then found in experiments designed with parameters demanded by the model (Leisner et al. 2010). It includes the Lehmann model as a special case.

The model works best if some oxidation occurs during the etching, the current density is not too low (a minimum spatial density of pores, for allowing interactions is required), and the oxide dissolution rate is not too fast. Thus, while it is presently the most general model, it is not a fully general model, but some of its postulates can be used independently to explain some phenomena.

The CBM allows computer simulation of pore growth. In this context, the first (and much simpler) model to allow computational simulations of pore morphology was the one proposed by Smith and Collins (Smith et al. 1988). The model deals with pore branching. It is based on the model of diffusion limited aggregation (DLA) by Witten and Sander (1983). The pore branching is explained by the random diffusion of electronic holes through depleted Si to the active etching sites.

Another important model is proposed by Parkhutik and Shershulsky (1992). It explains nucleation, pore growth, and rearrangements of the pore structure when changing the applied electric field. It has the following postulates:

- A virtual passive layer (VPL) covers the bottom of the pores. It avoids a direct contact of the electrolyte with Si.
- Pores are formed by electrochemical dissolution of the VPL. The charge transfer for the process can be tunneling through the VPL, or polarization of the VPL, which enhances the dissolution.
- The VPL growth and dissolution has an exponential dependency on the electric field strength, and it is influenced by the reactivity with the electrolyte and by other experimental variables.

The model considers a linear relationship between the pore size and the applied voltage or current. It also has a parameter containing information about the dependence of the pore diameter on the type of electrolyte. The calculation with the model results in a porosity parameter. Depending on the value of this parameter, six different pore morphologies are predicted. It is clear that this model puts parts of what should be explained into its assumptions and thus does not have much explanatory or predictive power.

2.4.2 FORMATION OF PORES WITH DIFFERENT DIAMETERS

In last section, models for porosification were discussed in general. Talking about the particular cases of micropores, mesopores, and macropores, all of these pores have some particularities that are not necessarily related to their diameter scale. Specific aspects of the different models can be used for describing the specific aspects of the different pore categories. Nevertheless, there is no model fully explaining pore formation in all diameter scales; combination of models must be used for having a plausible explanation. In what follows, the CBM and the SCR models will be used for describing pore formation.

A problem for having just one model describing all kinds of pores is that there is no continuity in sizes when varying the current density or doping concentration. For example, in *p*-type Si, macropores are typically obtained at $J << J_{PSL}$, low HF concentrations (in the range of 5%), and relatively high Si resistivities (generally larger than 1 Ω·cm). Mesopores are obtained at $J \sim J_{PSL}$ and high HF concentrations (in the range of 30%), on very low resistive Si. Micropores, on the other hand, are obtained at $J <\approx J_{PSL}$, large HF concentrations (in the range of 30%), and low Si resistivities. It can be stated, in a very simplified way, that etching of *n*+ and *p*+ Si under almost all conditions always results in mesopores.

As an example, Figure 2.5 shows the I-V characteristics of *p*- and *n*-type Si in HF-based aqueous electrolytes, denoting the different kinds of pores that can be obtained (Föll 2015): (A) micropores, (B) mesopores, (C) macropores, and (D) breakthrough pores. The last category refers to macropores, in principle, according to their diameter; however, their formation mechanism is different. They are obtained at potentials of dielectric breakdown.

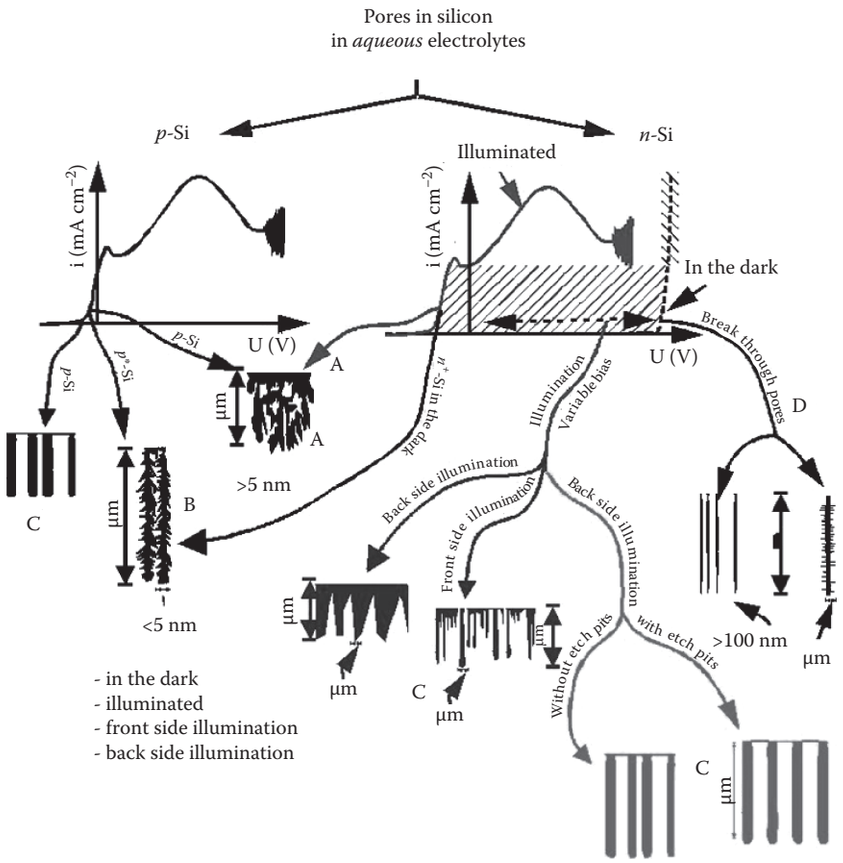

FIGURE 2.5 Morphologies of pores that can be obtained depending on the doping type and doping level, besides the operational point (particular I-V conditions).

2.4.2.1 MACROPORES

According to the CBM, macropores occur when sizable domains are possible (correlations in space and time happen). A decisive factor for this is that the SCRLs of the pores are close to each other. The minimum distance between pores is given by 2SCRL; under this condition, there are theoretically no carriers flowing to the pore walls. Thus, they are passivated. However, Grüning et al. (1996) has shown that even when the distance between pores is larger than 2SCRL, the current flows preferentially at the pore tips. This would mean that there are other passivation mechanisms of the pore walls, besides the SCRL, and that is the hydrogen (or hydrogen-bearing molecules) passivation discussed before. Even though, experimentally, the distance between pores cannot be increased without limit, if the distance is too small, some pores stop growing, and if it is too large, the pore surface becomes rough or the pore branches.

In Figure 2.6, it is possible to observe how macropores are usually distributed, when they nucleate by self-organization (Föll et al. 2010). For the mechanism of nucleation, please refer to Section 2.4.1.1. The distance between pores is usually not larger than the sum of the pore diameter d_{pore} plus 4SCRL. Additionally, the pores tend to close-pack (hexagonal array). Figure 2.7 shows an SEM micrograph of macropores in *n*-type Si with a self-organized hexagonal pattern. These pores are unusual and were predicted using the CBS model. They exhibit what is known as a frustrated structure—they want to assume a square lattice because of the crystal orientation constraints and a hexagonal lattice in order to be close-packed at the same time—an obvious impossibility. Thus, no particular order is visible to the naked eye. The inset, showing the FFT of the image, however, clearly shows that while there is indeed no correlation in space between nearest neighbors, there is a clear hexagonal structure for the second-nearest one.

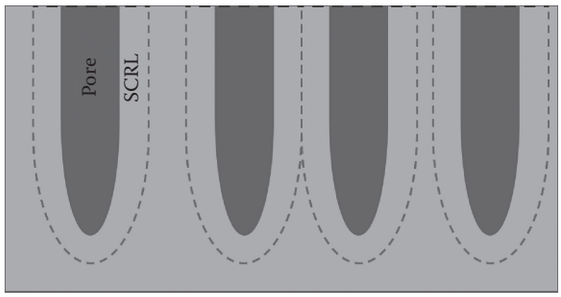

FIGURE 2.6 Schematic of the spatial distribution of macropores grown wild. The distance between pores is usually smaller than d_{pore} + 4SCRL.

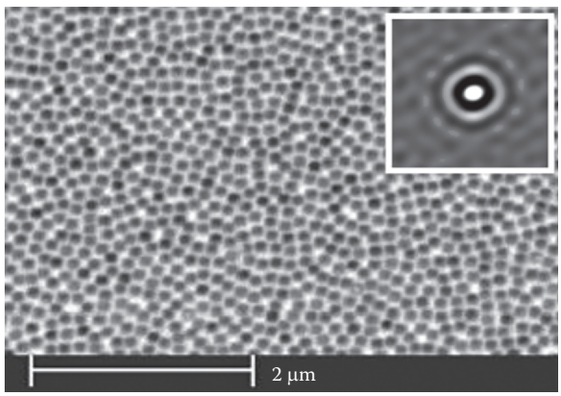

FIGURE 2.7 SEM micrograph of the surface of a macroporous Si sample with pores grown wild. The pores tend to grow close-packed. The inset shows the FFT of the micrograph, evidencing a predominantly hexagonal muster.

If the Si surface is prepatterned with an array of inverted pyramids, the pores tend to grow exactly at the positions of the pyramid tips because the probability of nucleation at those points is enhanced (the electric field strength is larger there). The pores stay at those positions without branching if the distance between pyramids is not larger than d_{pore} + 4SCRL. Furthermore, if the distance between pyramids is close to 2SCRL (as in Figure 2.8), the pore walls are well passivated, and their roughness is low because there is no current flow to them. d_{pore} is allowed to vary if there is available space between the SCRLs of contiguous pores.

For etching macropores in *n*-type Si, photogeneration of holes is needed because the majority carriers are electrons, but holes are necessary for the dissolution reaction of Si. Backside illumination is preferred over frontside illumination because the diffusion of carriers to the pore tips has to go down into the sample and the current-focusing effect of the pore tip is lost. Pores obtained by frontside illumination thus are limited as to their depths. Pores in *n*-type Si can, within certain

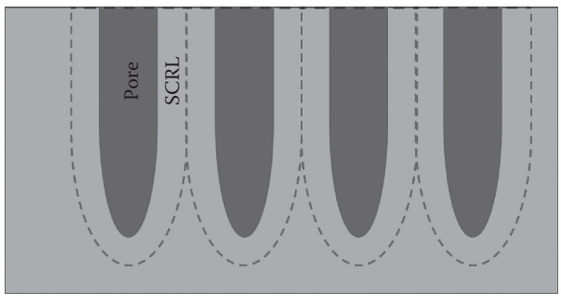

FIGURE 2.8 Schematic of the spatial distribution of macropores grown on pre-patterned Si. The minimum distance between pores is 2SCRL.

limits, be well predicted through the Lehmann model, described by Equation 2.8. According to the model, it is possible to vary the diameter of the pores by varying the applied current. Working at the operational point for PSL (see the *J-V* characteristics of Figure 2.3), the pore diameters adjust themselves to keep the current density at the level of J_{PSL}.

Working with *n*-type Si has the advantage that one can vary the photocurrent (via the intensity of the applied light) and the voltage simultaneously. This gives an additional degree of freedom. Figure 2.9 shows typical photocurrent and voltage profiles for making a cavity. Figure 2.10 (solid line) indicates the shape of pores obtained with those profiles. It is expected that if the chemical processes are fast enough to follow changes of current, diameter modulations could be obtained (as described by the dashed line of Figure 2.10). However, it has been considered a difficult task for many years because the already-etched pores were always over-etched while etching deeper, and no clear modulations could be observed (Müller et al. 2000). Nevertheless, Matthias et al. (2005), taking advantage of being able to vary voltage and current independently, reported the first macropores with sharp modulations. Figure 2.11 shows possible photocurrent and voltage profiles for accomplishing the expected pores of Figure 2.10.

In the case of *p*-type Si, the etching is relatively isotropic and it is difficult to achieve pore modulation due to the large availability of electronic holes, even though Christophersen et al. (2000b) finally found very stable growth conditions for p-type macropores, using organic electrolytes. They could grow pores as deep as 400 μm. Furthermore, adding some surfactants like polyethyleneglycol (PEG), the surface is passivated, enhancing the focusing effect at the pore tips (Quiroga-González et al. 2014). In this way, in *p*-type Si it is possible to obtain the same structures than in *n*-type Si; in fact, pore modulation in *p*-type Si adding surfactants has allowed the fabrication of arrays of microwires with an intergrown support (Quiroga-González et al. 2011). Figure 2.12 shows an example of modulated macropores in *p*-type Si, prepared using PEG simply varying the current density.

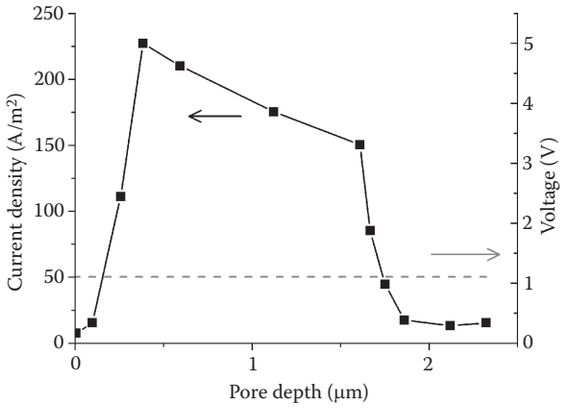

FIGURE 2.9 Common etching current and voltage profiles for making a pore modulation in *n*-type Si. In this case, just the photocurrent (light intensity) is varied, as one does for *p*-type Si.

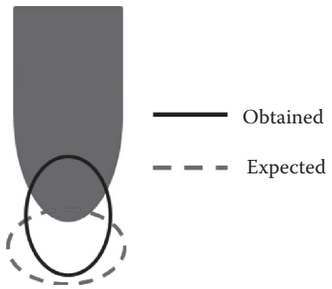

FIGURE 2.10 Schematic of pore obtained with the etching profiles of Figure 2.8. A modulation is obtained, but not as pronounced as desired (see dashed line).

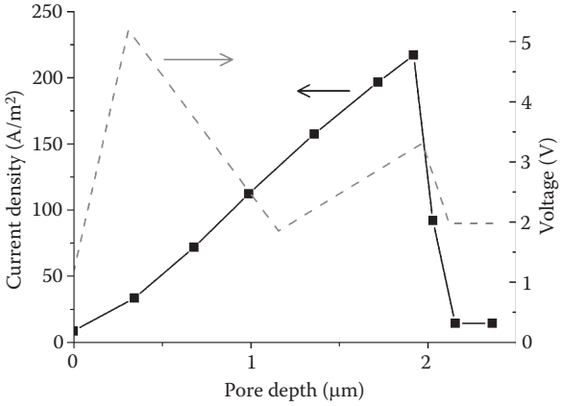

FIGURE 2.11 Optimized etching current and voltage profiles for making a pore modulation in *n*-type Si. Varying both the current and the voltage, it is possible to enhance the modulation, and pores close to the ones of Figure 2.9 (expected) can be obtained.

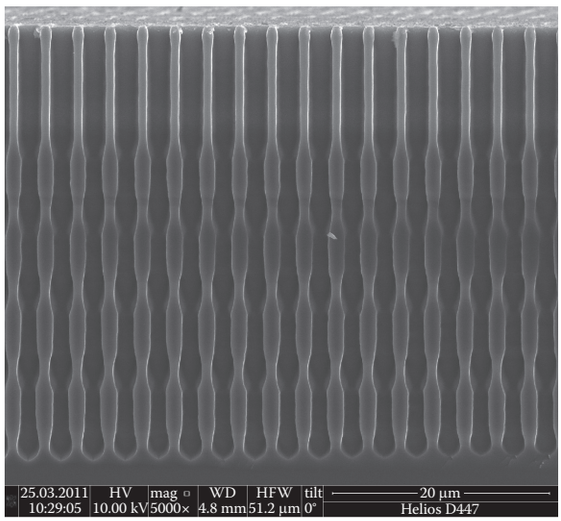

FIGURE 2.12 SEM of modulated macropores in *p*-type Si. A good contrast between wide and narrow sections is possible by enhancing the passivation of the pore walls with surfactants.

Exhaustive experimental work has shown that macropores in *n*- and *p*-type Si grow preferentially in <100> directions, but when the available <100> directions are too inclined, they grow in <113> directions (Rönnebeck et al. 2000; Christophersen et al. 2000b,c). The main pores usually grow in one of these directions, and may branch in some of the others. Only the CBS model is able to account for this peculiar behavior in a qualitative way.

2.4.2.2 MESOPORES

The pore growth mechanism in this kind of pore, quite different from the others, is that charge transfer for the etching process is given by barrier breakdown, for example, by tunneling (Zhang 2001). According to the CBM, these pores are produced by a positive interaction of CBs in time without the formation of synchronized domains, and a low interaction in space. The lack of domains is an indication of insufficient oxidation. The etching process is mainly produced by direct dissolution.

Mesopores can be directly prepared either in *p*- or in *n*-type Si with different doping or as by-product during the preparation of other pores:

- The most common way of preparation of mesopores is using highly doped *p*-type Si in aqueous electrolytes (Sailor 2012). In the case of the highly doped *n*-type material no illumination is required, contrary to what one expects in macropore formation, because there is enough current produced by avalanche break-down (Lehmann et al. 2000). Due to the low resistivity, this kind of process is easy to accomplish, even at small voltages. Etching in organic electrolytes also works, even at lower doping concentrations (Carstensen et al. 2000; Christophersen et al. 2000d). It seems that weak oxidizing electrolytes promote mesopore formation: As the thickness of the oxide is very small, the probability of carrier tunneling is high, and direct dissolution of Si is produced.
- Using moderately doped *n*-type Si, mesopores can be produced, too. Under darkness conditions, when high voltages are applied (as high as 100 V), dielectric breakdown occurs producing mesopores.
- Additionally, mesopores can be found on the walls of macropores grown in *n*- or *p*-type Si, using weak oxidizing electrolytes (mainly organic). This also happens when macropores stop growing (Jäger et al. 2000).

Carstensen et al. 2000 is not in the References section. Please provide complete publication details.

2.4.2.3 MICROPORES

This kind of pore occurs when an anticorrelation between nucleation points occurs. The formation of pores is also enhanced by quantum dot effects. According to the CBM, an anticorrelation happens when the nucleation probability at a certain point (x, y) gets its maximum when no previous CB has occurred there. In this case, pore nucleates as soon as possible in reduced areas, right after oxide dissolution. In this case, the current density of a CB is very large, forming pores with a sponge-like structure.

While the CBM explains the probability of micropore formation, there are no models fully explaining their growth, diameter, and morphology. For example, the model of the quantum wire effect only accounts for the distance between pores (Lehmann and Gösele 1991).

Micropores are usually obtained using large HF concentrations and high currents. This allows fast pore growth and high porosity (Lehmann 1993). If the HF concentration or the current densities are too low, macropores are produced. On the other hand, the doping concentration for obtaining micropores is usually low, as in the case of macropores. Micropores can be obtained equally in *n*- or *p*-type Si, low doped. If the doping increases, mesopores are obtained. In this way, one can situate micropores between macropores and mesopores in a phase diagram for pores. A qualitative phase diagram is shown in Figure 2.13. Here, the most common ways for preparing the different kinds of pores are presented. Transitions between pore types are possible.

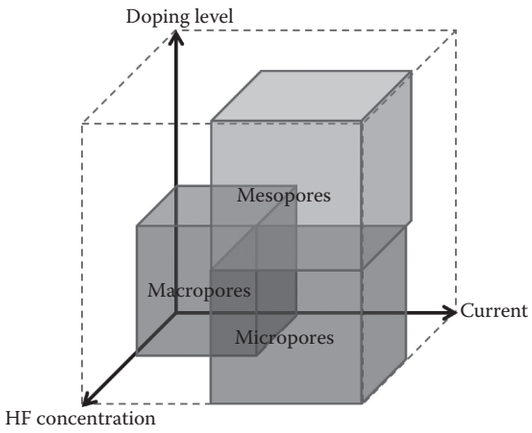

FIGURE 2.13 General phase diagram of pores. In this graph, the most common ways of obtaining the different dimensions of pores are depicted. The three most important parameters influencing the pore size (HF concentration, doping level, and current density) are the axes.

2.5 SUMMARY

The *J-V* (current density–voltage) characteristics of the electrochemical etching system of Si behave in a first approximation like a rectifying metal-semiconductor contact, generally known as a Schottky contact. Nevertheless, the characteristics present some features not seen in a solid state. At negative potentials, H_2 evolution occurs, independently if one etches *p*- or *n*-type Si. At positive potentials, Si dissolution is observed, but for the case of *n*-type Si, illumination has to be applied (the dissolution process requires electronic holes, which are not available in the *n*-type material in dark). Below a current density value JPSL (current density for porous Si layer), pores are obtained. Beyond this current, electropolishing occurs. Electrochemical etching of Si with HF-based solutions consists of any combinations of four processes: direct dissolution of Si, oxidation of Si, dissolution of the Si oxides, and hydrogen passivation.

According to IUPAC, pores can be grouped into micropores (diameter <2 nm), mesopores (diameter 2–50 nm), and macropores (diameter >50 nm). There are different models trying to explain pore formation. These can be grouped in models for pore nucleation, for steady pore growth, or for the whole pore formation. Among these models, the current burst model (CBM) is one of the most complete, allowing prediction and modeling of pores, and the Lehmann model, explaining steady growth of macropores, based on the fact of pore wall passivation by a space charge region lager.

Micropores are usually obtained using large HF concentrations, high currents, and low doping, by direct dissolution or oxide formation and its dissolution. Mesopores are obtained by tunneling of carriers, using large HF concentrations, high currents, and high doping. Macropores are obtained by a similar mechanism as micropores, but using low HF concentrations, low currents, and low doping.

REFERENCES

Anglin, E.J., Cheng, L., Freeman, W.R., and Sailor, M.J. (2008). Porous silicon in drug delivery devices and materials. *Adv. Drug Deliv. Rev.,* **60**, 1266–1277.

Beale, M.I.J., Chew, N.G., Uren, M.J., Cullis, A.G., and Benjamin, J.D. (1985). Microstructure and formation mechanism of porous silicon. *Appl. Phys. Lett.,* **46**(1), 86–88.

Canham, L.T. (1990). Silicon quantum wire fabrication by electrochemical and chemical dissolution of wafers. *Appl. Phys. Lett.,* **57**(10), 1046–1048.

Carstensen, J., Prange, R., Popkirov, G.S., and Föll, H. (1998). A model for current oscillations at the Si-HF-System based on a quantitative analysis of current transients. *Appl. Phys. A,* **67**, 459–467.

Carstensen, J., Prange, R., and Föll, H. (1999). A model for current-voltage oscillations at the silicon electrode and comparison with experimental results. *J. Electrochem. Soc.,* **146**(3), 1134–1140.

Chabal, Y.J., Chaban, E.E., and Christman, S.B. (1983). High resolution infrared study of hydrogen chemisorbed on Si(100). *J. Electron. Spectrosc. Relat. Phenom.,* **29**, 35–40.

Christophersen, M., Carstensen, J., Feuerhake, A., and Föll, H. (2000a). Crystal orientation and electrolyte dependence for macropore nucleation and stable growth on *p*-type-silicon. *Mater. Sci. Eng. B,* **69/70**, 194–198.

Christophersen, M., Carstensen, J., and Föll, H. (2000b). Crystal orientation dependence of macropore formation in *p*-type silicon using organic electrolyte. *Phys. Stat. Sol. (a),* **182**(1), 103–107.

Christophersen, M., Carstensen, J., and Föll, H. (2000c). Crystal orientation dependence of macropore formation in *n*-type silicon using organic electrolyte. *Phys. Stat. Sol. (a),* **182**(2), 601–606.

Christophersen, M., Carstensen, J., and Föll, H. (2000d). Macropore formation on highly doped *n*-type silicon. *Phys. Stat. Sol. (a),* **182**(1), 45–50.

Christophersen, M., Carstensen, J., Rönnebeck, S., Jäger, C., Jäger, W., and Föll, H. (2001). Crystal orientation dependence and anisotropic properties of macropore formation of *p*- and *n*-type silicon. *J. Electrochem. Soc.,* **148**(6), E267.

Corbett, J.W., Shereshevskii, D.I., and Verner, I.V. (1995). Changes in the creation of point defects related to the formation of porous silicon. *Phys. Stat. Sol. (a),* **147**, 81–89.

Föll, H. (1991). Properties of silicon-electrolyte junction and their application to silicon characterization. *Appl. Phys. A*, **53**, 8–19.

Föll, H. (2015). Macroporous silicon. http://www.tf.uni-kiel.de/matwis/amat/. Accessed on January 20, 2015.

Föll, H., Christophersen, M., Carstensen, J., and Hasse, G. (2002). Formation and application of porous silicon. *Mater. Sci. Eng. R.,* **39**(4), 93–141.

Föll, H., Carstensen, J., and Frey, S. (2006). Porous and nanoporous semiconductors and emerging applications. *J. Nanomat.,* **91635**, 1–10.

Föll, H., Leisner, M., Cojocaru, A., and Carstensen, J. (2010). Macroporous semiconductors. *Materials,* **3**, 3006–3076.

Föll, H., Leisner, M., and Carstensen, J. (2011). Modeling some "meta" aspects of pore growth in semiconductors. *ECS Trans.,* **35**(8), 49–60.

Grüning, U., Ottow, S., Busch, K., and Lehmann, V. (1996). Macroporous silicon with a complete two-dimensional photonic band gap centered at 5 μm. *Appl. Phys. Lett.,* **68**(6), 747–749.

Hejjo Al Rifai, M., Christophersen, M., Ottow, S., Carstensen, J., and Föll, H. (2000). Dependence of macropore formation in *n*-Si on potential, temperature, and doping. *J. Electrochem. Soc.,* **147**(2), 627–635.

Hoffmann, P.M., Vermeir, I.E., and Searson, P.C. (2000). Electrochemical etching of *n*-type silicon in fluoride solutions. *J. Electrochem. Soc.,* **147**(8), 2999–3002.

Huang, Z., Geyer, N., Werner, P., de Boor, J., and Gösele, U. (2011). Metal-assisted chemical etching of silicon: A review. *Adv. Mater.,* **23**, 285–308.

Jäger, C., Finkenberger, B., Jäger, W., Christophersen, M., Carstensen, J., and Föll, H. (2000). Transmission electron microscopy investigations of the formation of macropores in *n*- and *p*-Si(001)/(111). *Mater. Sci. Eng. B,* **69/70**, 199–204.

Kang, Y. and Jorné, J. (1993). Morphological stability analysis of porous silicon formation. *J. Electrochem. Soc.,* **140**, 2258–2265.

Kochergin, V. and Föll, H. (2009). *Porous Semiconductors: Optical Properties and Applications*. Springer, Berlin.

Kompan, M.E., Kuzminov, E.G., and Kulik, V. (1996). Observation of a compressed state of the quantum wire material in porous silicon by the method of Raman-scattering. *JETP Lett.,* **64**(10), 748–753.

Lehmann, V. (1993). The physics of macropore formation in low doped *n*-type silicon. *J. Electrochem. Soc.,* **140**(10), 2836–2843.

Lehmann, V. (2002). *Electrochemistry of Silicon*. Wiley-VCH, Weinheim.

Lehmann, V. and Föll, H. (1990). Formation mechanism and properties of electrochemically etched trenches in *n*-type silicon. *J. Electrochem. Soc.,* **137**(2), 653–659.

Lehmann, V. and Gösele, U. (1991). Porous silicon formation: A quantum wire effect. *J. Appl. Phys. Lett.,* **58**(8), 856–858.

Lehmann, V. and Grüning, U. (1997). The limits of macropore array fabrication. *Thin Solid Films,* **297**(1–2), 13–17.

Lehmann, V., Stengl, R., and Luigart, A. (2000). On the morphology and the electrochemical formation mechanism of mesoporous silicon. *Mater. Sci. Eng. B,* **69/70**, 11–22.

Leisner, M., Carstensen, J., and Föll, H. (2010). Pores in *n*-type InP: A model system for electrochemical pore etching. *Nanoscale Res. Lett.,* **5**, 1190–1194.

Mathwig, K., Geilhufe, M., Müller, F., and Gösele, U. (2011). Bias-assisted KOH etching of macroporous silicon membranes. *J. Micromech. Microeng.,* **21**, 035015.

Matthias, S., Müller, F., Schilling, J., and Gösele, U. (2005). Pushing the limits of macroporous silicon etching. *Appl. Phys. A,* **80**(7), 1391–1396.

Müller, F., Birner, A., Schilling, J., Gösele, U., Kettner, C., and Hänggi, P. (2000). Membranes for micropumps from macroporous silicon. *Phys. Stat. Sol. (a),* **182**(1), 585–590.

Parkhutik, V. (1999). Porous silicon—Mechanisms of growth and applications. *Solid State Electron.,* **43**, 1121–1141.

Parkhutik, V.P. and Shershulsky, V.I. (1992). Theoretical modeling of porous oxide growth on aluminium. *J. Phys. D.,* **25**(8), 1258–1263.

Parkhutik, V. and Andrade Ibarra, E. (1999). The role of hydrogen in the formation of porous structures in silicon. *Mater. Sci. Eng. B.,* **58**, 95–99.

Propst, E.K. and Kohl, P.A. (1994). The electrochemical oxidation of silicon and formation of porous silicon in acetonitrile. *J. Electrochem. Soc.,* **141**(4), 1006–1013.

Propst, E.K., Rieger, M.M., Vogt, K.W., and Kohl, P.A. (1994). Luminescent characteristics of a novel porous silicon structure formed in a nonaqueous electrolyte. *Appl. Phys. Lett.,* **64**(15), 1914–1916.

Quiroga-González, E., Ossei-Wusu, E., Carstensen, J., and Föll, H. (2011). How to make optimized arrays of Si wires suitable as superior anode for Li-ion batteries. *J. Electrochem. Soc.,* **158**(11), E119–E123.

Quiroga-González, E., Carstensen, J., Glynn, C., O'Dwyer, C., and Föll, H. (2014). Pore size modulation in electrochemically etched macroporous *p*-type silicon monitored by FFT impedance spectroscopy and Raman scattering. *Phys. Chem. Chem. Phys.,* **16**, 255–263.

Rönnebeck, S., Ottow, S., Carstensen, J., and Föll, H. (2000). Crystal orientation dependence of macropore formation in *n*-Si with backside-illumination in HF-electrolyte. *J. Por. Mat.,* **7**(1–3), 353–356.

Sailor, M.J. (2012). *Porous Silicon in Practice*. Wiley-VCH, Weinheim.

Smith, R.L., Chuang, S.-F., and Collins, S.D. (1988). A theoretical model of the formation morphologies of porous silicon. *J. Electron. Mater.,* **17**(6), 533–541.

Witten, T.A. and Sander, L.M. (1983). Diffusion-limited aggregation. *Phys. Rev. B.,* **27**(9), 5686–5697.

Yavlonovitch, E., Allara, D.L., Chang, C.C., Gmitter, T., and Bright, T.B. (1986). Unusually low surface recombination velocity on silicon and germanium surfaces. *Phys. Rev. Lett.,* **57**(2), 249–252.

Zhang, X.G. (1991). Mechanism of pore formation on *n*-type silicon. *J. Electrochem. Soc.,* **138**(12), 3750–3756.

Zhang, X.G. (2001). *Electrochemistry of Silicon and Its Oxide*. Kluwer Academic—Plenum Publishers, New York.